Journal of Southeast University (English Edition) Vol. 25, No. 1, pp. 41 – 46 Mar. 2009 ISSN 1003—7985

Design and analysis of a bisected wheel-based cable climbing robot

Xu Fengyu Wang Xingsong Xu Jialin

(School of Mechanical Engineering, Southeast University, Nanjing 211189, China)

Abstract: To inspect inner wires of the cylindrical cables on a cable-stayed bridge, a new bisected wheel-based cable climbing robot is designed. The simple structure and the moving mode are described and the static features of the robot are analyzed. A cable with a diameter of 139 mm is selected as an example to calculate the design parameters of the robot. For safety energy-saving landing in the case of electrical system failure, an electric damper based on back electromotive force and a gas damper with a slider-crank mechanism are introduced to exhaust the energy generated by gravity when the robot is slipping down along the cables. A simplified mathematical model is analyzed and the landing velocity is simulated. For the present design, the robot can climb up a cable with diameters varying from 65 to 205 mm with payloads below 3.5 kg. Several climbing experiments performed on real cables confirm that the proposed robot meets the demands of inspection.

Key words: climbing robot; energy-saving landing; gas damper; cable; cable-stayed bridge

Climbing robots have various applications in industry and hazardous environments. Inspection of high chimneys, vertical and inclined pipes in nuclear power plants, and wiring on high voltage power transmission towers are some well known examples of such applications[1–3]. Moreover, there are some new and other important tasks for these robots, for instance, examining cables on a cable-stayed bridge[4–5].

Cable is one of the most important stress components of the cable-stayed bridges. In the United States, several cable-stayed bridges have shown signs of cable damage mostly induced by susceptibility of stay cables to wind-induced vibrations and corrosion[6]. This has caused public concerns and initiated a series of inspection and security monitoring programs. The cables must be examined periodically to ensure the reliability of the bridge. For a long time, the inspection has been conducted artificially, which is inefficient and dangerous. Under these circumstances, a new wheel-based cable climbing robot is proposed for cable inspection usage.

Climbing robots belong to a specialized field of mobile robots. The main feature is the mobility against the gravity of the body. An important aspect to consider in the design of such robots is that they need to be lightweight and powerful enough to move up to support their own weight[7]. Therefore, the designer should consider not only the locomotion method, as in conventional mobile robots, but also the techniques involved in sticking to the cable. There are several forms of adhesion methods:

1) Magnetic mechanisms for climbing on ferrous surfaces via electromagnets or permanent magnets[8];

2) Vacuum suction technologies for sticking the robot on the walls[9–10];

3) Grippers or armed mechanisms that attach to the structure such as beams, columns, pipes and tubes[11].

According to the modes of locomotion, climbing robots can be classified into three main groups:

1) Wheel-driven machines climb vertical planes by combining wheels for translation, and by magnets or vacuum suction for surface attachment[12];

2) Legged climbing robots[13] consist usually of four or six legs, each of them with magnets or a vacuum pump for attachment but with limited maneuverability;

3) Locomotion based on arms with grippers or other devices that provide the robot with skillful mobility[14].

The climbing robot proposed in this paper utilizes a spring to provide friction forces to support the whole robotic system. With the driving wheel actuated by a powerful DC motor, the robot can climb on a cable inclined at any angle, including a vertical one. Another important advantage of the robot over other climbing robots is that it is fail-safe because it possesses a landing mechanism to ensure that the robot returns safely in the case of electrical system failure.

1 Structure of the Robot

Unlike our previously designed climbing robot which was a trisected robot[15], there are several improvements introduced here. The first improvement is that the climbing robot (shown in Fig. 1) is composed of two equally spaced modules facing each other. Only one of the two modules is powered and the other is passive. Each module possesses two wheel limbs at the two ends. Only the upper wheel of the powered module is actuated by a DC motor. The passive

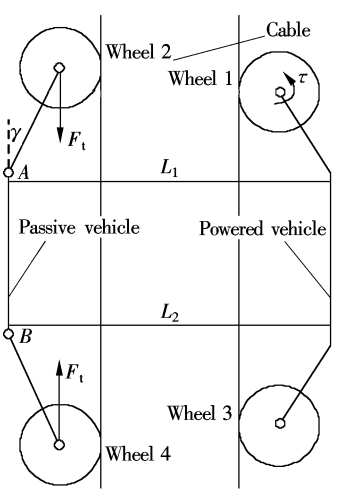

Fig. 1 The structure of cable inspection robot

Received 2008-05-23.

Biographies: Xu Fengyu (1979—), male, graduate; Wang Xingsong (corresponding author), male, doctor, professor, xswang@seu.edu.cn.

Foundation item: The National High Technology Research and Development Program of China (863 Program) (No. 2006AA04Z234).

Citation: Xu Fengyu, Wang Xingsong, Xu Jialin. Design and analysis of a bisected wheel-based cable climbing robot[J]. Journal of Southeast University (English Edition), 2009, 25(1): 41 – 46.

module is applied to provide the supporting force to increase system stability.

The two modules are joined by eight connected bars (L_1, L_2) to form a whole closed hexagonal body to clasp the cable. By changing the joined holes of the connecting bars, the robot can climb cables with various diameters. All the wheels (including the driving wheel) are machined in V-shape with an open angle $\phi = 150°$ to increase area of contact. This can also reduce abrasion, prevent the driving wheel from deflecting off the cable, and avoid getting stuck. The wheel limbs of the passive module are connected with an extension spring to provide the robot with enough clasping force F_t. The limbs are hinged to the body of the passive modules at A, B, which enable the robot to climb over small obstacles by the elongation of the spring. In order to reduce the drag force and to ensure that only one wheel crawls on an obstacle at a time, the passive wheel is offset from the driving wheel by a distance of 10 mm.

In the case of power shortage or electrical failure, in order to ensure that the robot safely slips down due to its own gravity, there is also a safe landing mechanism attached to the driving wheel through a one-way clutch. This is the second improvement. The principle of the landing mechanism will be discussed in detail in section 3.

An encoder is applied to measure the distance the robot has climbed. There is a moustache sensor to detect the top end of the cable. When it arrives at the top end, the driving motor will be powered off and the robot will slip downward by its own gravity. At this time the safe landing mechanism will work to ensure that the robot safely lands without consuming any energy.

2 Static Features Analysis

Fig. 2(b) is the top view of the climbing mechanism. The upper wheels are called wheel 1 and wheel 2, while the lower wheels are called wheel 3 and wheel 4, respectively. Suppose N_{i1} and N_{i2} (i is the serial number of the wheel) are the forces the cable acting on the two contacting points of wheel i, and N_i are the resultant forces of N_{i1} and N_{i2}. Then

$$N_i = N_{i1}\sin\frac{\phi}{2} + N_{i2}\sin\frac{\phi}{2} \tag{1}$$

The direction of the resultant force is perpendicular to the axes of the wheels. F_{fi1} and F_{fi2} are the rolling frictional resistance that the cable acts on the two points of wheel i.

As the wheels are identical, according to the symmetrical characteristics of the passive wheels and the symmetrical arrangement, one can obtain

$$\left.\begin{aligned} F_{fij} &= N_{ij}\mu_1 \qquad i \neq 1 \\ F_{fi} &= F_{fi1} + F_{fi2} = N_{i1}\mu_1 + N_{i2}\mu_1 \end{aligned}\right\} \tag{2}$$

where f_{fi} is the resultant force of F_{fi1} and F_{fi2}, the direction is along the cable, and μ_1 is the coefficient of rolling friction.

All the forces acting on the robot system are shown in Fig. 2. Assume that the two modules are the same in clamping the cable and are the same in support of the loads and their own gravities. One can obtain the following equilibrium equations.

In the plane of xz, we can obtain

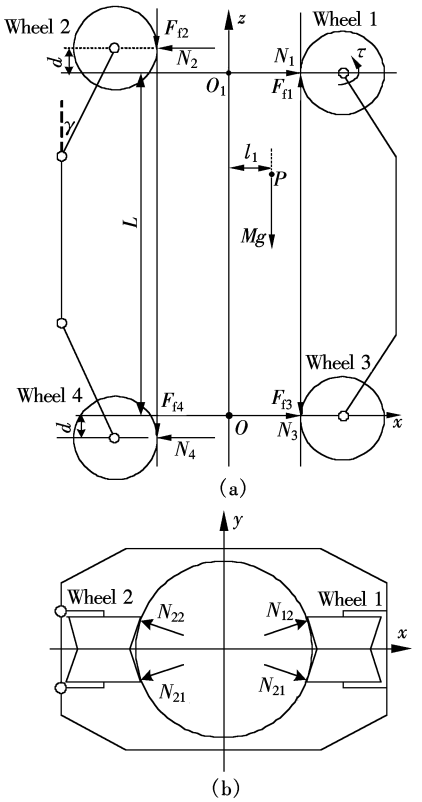

Fig. 2 View of the climbing mechanism

$$\sum X = N_1 + N_3 - N_2 - N_4 = 0 \tag{3}$$

$$\sum Z = F_{f1} - Mg - F_{f4} - F_{f2} - F_{f3} \tag{4}$$

For moment-equilibrium,

$$M_{o1}(F) = \tau - mgl_1 + \sum_{i=1}^{4} M_{o1}(N_{i1}) + \sum_{i=1}^{4} M_{o1}(N_{i2}) + \sum_{i=1}^{4} M_{o1}(F_{fi1}) + \sum_{i=1}^{4} M_{o1}(F_{fi2}) = 0 \tag{5}$$

where τ is the output torque of the driving motor, P is the gravity center of the mechanism, r is the radius of the cable, d is the eccentric distance from the passive wheel to the driving wheel, and l_1 is the eccentric distance of the gravity center.

The force diagrams of wheel 2 and wheel 4 are shown in Fig. 3(a) and Fig. 3(b), respectively.

$$\left.\begin{aligned} F_2\cos\gamma &= F_t + m_{w2}g + F_{f2} \\ F_2\sin\gamma &= N_2 = 2N_{21}\cos 15° \end{aligned}\right\} \tag{6}$$

$$\left.\begin{aligned} F_t &= F_4\cos\gamma + F_{f4} + m_{w4}g \\ F_4\sin\gamma &= N_4 = 2N_{41}\cos 15° \end{aligned}\right\} \tag{7}$$

The diagram of the driving wheel is shown in Fig. 3(c).

$$\tau = F_{f1}r_1 \tag{8}$$

where γ denotes the angle between the limb and the body, $m_{wi}g$ is the gravity force of wheel i, F_t is the pulling force of the spring, F_i is the supporting force acting on the wheels, and r_1 is the effective radius of the driving wheel.

From Eqs. (3) and (4),

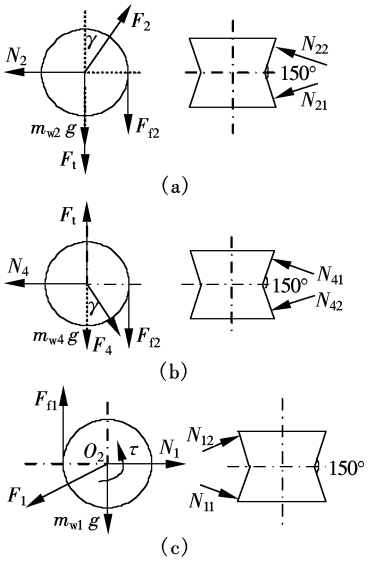

Fig. 3 Force diagram of the wheels

$$F_{f1} = 2F_{f11} = Mg + 2N_{21}\mu_1 + 2N_{31}\mu_1 + 2N_{41}\mu_1 \quad (9)$$

According to Eqs. (6), (8) and (9),

$$N_{31} = \frac{Mg(l_1 - r_1 - r\cos 15°) - 2N_{21}B + 2N_{41}C}{2A} \quad (10)$$

where

$$A = \mu(r_1 + r\cos 15°) + \cos 15°(L - \mu_1 r)$$
$$B = \mu_1(r_1 + r\cos 15°) + \cos 15°(d + \mu_1 r)$$
$$C = \cos 15°(L + d - \mu_1 r) - \mu_1(r_1 + r\cos 15°)$$

Therefore, when the robot is climbing at a uniform speed, the output torque of the DC motor is

$$\tau = F_{f1} r_1 = (Mg + 2N_{21}\mu_1 + 2N_{51}\mu_1 + 2N_{41}\mu_1) r_1 \quad (11)$$

Setting $2N_{11}\mu_2 > F_{f1}$, thus the mechanism satisfies the climbing condition. Take a ϕ139 mm cable as an example, the material of the driving wheel is aluminum coating with hard rubber and the passive wheels are MC nylon; Mg is the gravity of the robot and payload, L is the distance between wheel 1 and wheel 3, K is the stiffness coefficient of the spring, μ_2 is the static friction coefficient, γ is the angle between limb and body, $m_{wi}(i = 2, 3, 4)$ is the passive wheels' weight, and F_t is the pulling force of the spring.

3 Analysis of the Landing Mechanism

In this section, the second big improvement of the landing speed constraint mechanism is introduced. In order to make the robot land at a controllable velocity (the value is not too large) in the case of power shortage or electrical failure, the new designed robot has a falling speed control mechanism consisting of a pneumatic cylinder and a slider-crank mechanism whose crank is fixed with the driving shaft through a one-way clutch. While the robot is slipping down, the rotation motion of the driving wheel is transmitted to the piston's reciprocating motion in the pneumatic cylinder. The gas in the cylinder is inhaled or ejected alternately from the hole forming a gas damper to consume the kinetic energy of the robot. The size of the hole can be adjusted to obtain different dampers so as to control the landing speed of the robot.

The principle of the landing mechanism is shown in Fig. 4. A slider-crank mechanism is a single-looped mechanism, which has a constrained condition as follows:

$$\beta = \arcsin\left(\frac{r_2}{l}\sin\alpha\right) \quad (12)$$

The rotary inertia of the connecting rod is very small, so the connecting rod can be considered as a two-force member neglecting its reciprocation and rotation.

$$F_e = \frac{A(p_0 - p) - m_2 a}{\cos\beta}$$

For the crank, the angular velocity and the acceleration are

$$\left.\begin{aligned} w &= \frac{\mathrm{d}a}{\mathrm{d}t} \\ \varepsilon &= \mathrm{J}^{-1}(\tau - F_e r_2 \sin(\alpha + \beta)) \end{aligned}\right\} \quad (13)$$

where a is the acceleration of the piston and r_2 is the length of the crank.

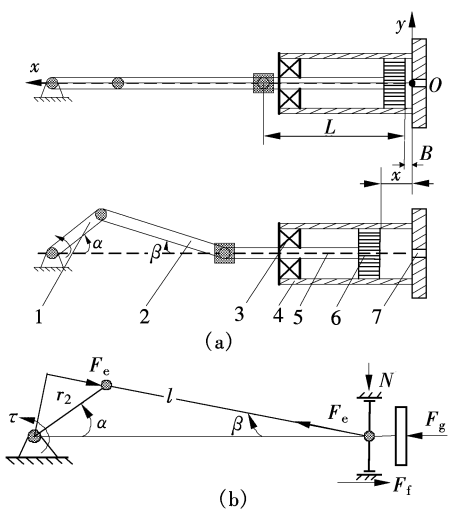

1—Crank; 2—Connecting rod; 3—Linear bearing; 4—Pneumatic cylinder; 5—Piston connecting rod; 6—Pistons; 7—Nozzle

Fig. 4 Landing mechanism

The displacement of the piston is

$$\left.\begin{aligned} x &= B + L + r_2 - r_2\left(\cos\alpha + \frac{\lambda}{4}\cos 2\alpha - \frac{\lambda}{4}\right) \\ \lambda &= \frac{r_2}{l} \end{aligned}\right\} \quad (14)$$

The speed and acceleration of the piston is as follows:

$$\left.\begin{aligned} v &= \frac{\mathrm{d}x}{\mathrm{d}t} = r_2 \frac{\mathrm{d}\alpha}{\mathrm{d}t}\left(\sin\alpha + \frac{\lambda}{2}\sin 2\alpha\right) \\ a &= \frac{\mathrm{d}v}{\mathrm{d}t} = r_2 w^2(\cos\alpha + \lambda\sin 2\alpha) \end{aligned}\right\} \quad (15)$$

When slipping down the cables, the robot accelerates at the beginning, and then fluctuates after the velocity achieves a fixed value. So the robot is in quasi-uniform motion, the

approximate torque acting on the crankshaft is

$$\tau_2 = r_2 Mg$$

The physical process involved in the emission and suction of gas is complex. To simplify the analysis, some assumptions are made: 1) The gas flows adiabatically in the cylinder and is isentropic at the release point; 2) The model of flow is considered as a one-dimensional model.

The value of the release rate in the hole depends on whether the gas flow is sonic or subsonic. This will be determined by the critical pressure ratio[16]:

$$H = \left(\frac{2}{1+k}\right)^{\frac{k}{k-1}} = 0.528$$

When $H \leqslant 0.528$, the gas release in the hole is a sonic flow. The release rate passing the orifice is described by the following equation:

$$Q = \mu A \mid p_1 \mid \sqrt{k \frac{M_1}{ZRT}\left(\frac{2}{1+k}\right)^{\frac{k+1}{k-1}}} \tag{16}$$

When $H > 0.528$, the gas release is subsonic, and the release rate is

$$Q = \mu A \mid p_1 \mid \sqrt{\frac{M_1}{ZRT}\frac{2k}{k-1}\left[\left(\frac{\mid p_0 \mid}{\mid p_1 \mid}\right)^{\frac{2}{k}} - \left(\frac{\mid p_0 \mid}{\mid p_1 \mid}\right)^{\frac{k+1}{k}}\right]} \tag{17}$$

The specific volume is

$$v = \frac{1}{\rho} = \frac{m}{V}$$

So the volume flow is

$$Q_1 = \begin{cases} \mu A_{or} \mid p_1 \mid v \sqrt{k \frac{M_1}{ZRT}\left(\frac{2}{k+1}\right)^{\frac{k+1}{k-1}}} \\ \mu A_{or} \mid p_1 \mid v \sqrt{\frac{M_1}{ZRT}\frac{2k}{k-1}\left[\left(\frac{\mid p_0 \mid}{\mid p_1 \mid}\right)^{\frac{2}{k}} - \left(\frac{\mid p_0 \mid}{\mid p_1 \mid}\right)^{\frac{k+1}{k}}\right]} \end{cases} \tag{18}$$

where A_{or} is the area of hole (m^2); μ is the empirical discharge coefficient (for subsonic gas of Reynolds number larger than 30 000, $\mu = 0.61$; for other situations $\mu = 1$); Q is the mass flux ($kg/(m^2 \cdot s)$); Q_1 is the release rate (kg/s), k is the heat capacity ratio; M_1 is the molecular weight ($kg/kmol$); p_1 is the pressure of the upstream (Pa); p_0 is the pressure in the cylinder (Pa); Z is the compression coefficient; R is the constant of gas ($Pa \cdot m^3/mol \cdot K$); T is the temperature of gas (K); ρ is the density of gas (kg/m^3); J is the inertia of the crank.

The pressure in the cylinder is influenced by two factors: 1) The variety of the cylinder's volume caused by the movement of the piston; 2) The gas has flowing through the hole caused by the pressure difference inside and outside of the cylinder.

$$P_t = P\left(\frac{V_0}{V_0 + \Delta V}\right)^k \pm P\left(\frac{\Delta C}{V_0 + \Delta V}\right)^k \tag{19}$$

where P_t is the instantaneous pressure after the movement of the piston and the gas has flowed; P is the instantaneous pressure; V_0 is the original volume; the value of ΔV, the variety of the volume caused by the piston, is positive when the volume is increasing, otherwise ΔV is negative; ΔC is the volume flow mentioned above.

One can simulate the landing velocity and the pressure in the cylinder through the analysis of the slider-crank mechanism and the gas cylinder. The experiments of the landing mechanism will be discussed in detail in the next section, including the method of the electric damper based on back electromotive force.

4 Simulation and Experimental Analysis

4.1 Simulation

The quasi-steady-state (QSS) simulation method is used to simulate the landing velocity of the mechanism. Fig. 5 is the simulation curve of the landing velocity and the pressure in the cylinder when the robot is slipping down from a 1.5 m high cable slanting 36°. The diameter of the testing cable is 139 mm. When reaching 0.287 m/s, the velocity begins to fluctuate at 0.25 m/s. The peak and valley of the wave is induced by different damping values caused by the varying pressures in the cylinder with the reciprocating movements of the piston. The mean speed will arise if the angle of the cable is larger, but the robot will not land as a freely falling body.

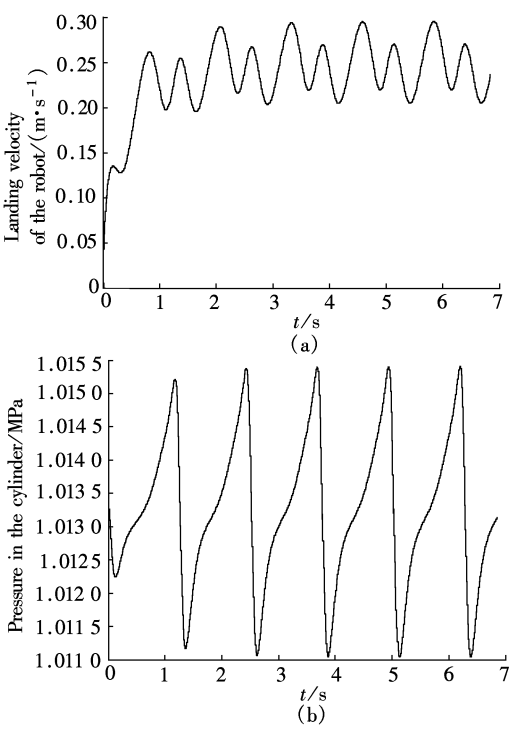

Fig. 5 Landing velocity and pressure in the cylinder. (a) Slipping velocity; (b) Pressure in the cylinder

4.2 Experiments in the laboratory

Various tests of movement are performed on horizontal, inclined and vertical cables. The smaller the cable's slanting angle is, the more difficultly the robot lands by deadweight. In general, the slanting angle of the cable in a cable-stayed bridge is not larger than 36°, so the cable is selected to test

the landing system. As shown in Fig. 6 , the robot climbs 1. 5 m then lands by various modes, so we can obtain the climbing velocity and the landing velocity.

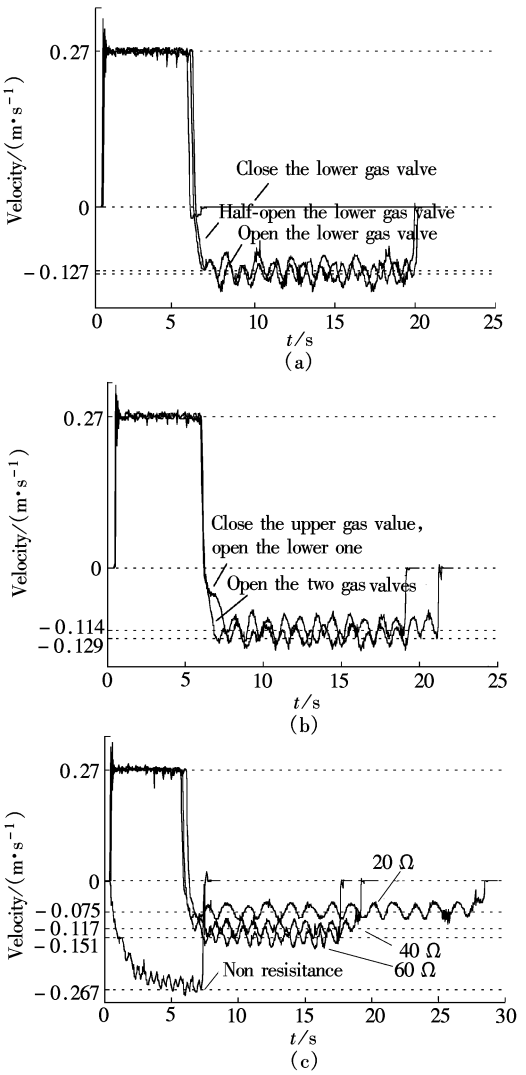

Fig. 6 The landing experiments of the robot. (a) The effect of the lower gas valve on landing velocity; (b) The effect of the upper gas valve on landing velocity; (c) The effect of the resistance on landing velocity

1) The effect of the lower gas valve on landing velocity

By inserting a 40 Ω resistance into the circuit and adjusting the lower gas valve, one can obtain three types of curves, as shown in Fig. 6(a).

The robot can land at 0 to 0. 127 m/s so as to realize stepless speed regulating. One disadvantage of the landing method is that we cannot control the hole of the gas valve and cannot obtain a precise velocity. But as a mechanical mode, with high reliability, the mechanism can restrict the landing speed effectively in the case of electricity system failure.

2) The effect of the upper gas valve on landing velocity

By inserting a 40 Ω resistance into the circuit and opening the lower valve, we can obtain two curves reflecting the landing velocity by adjusting the upper valve to two limit states, as shown in Fig. 6(b). So one can conclude that the upper valve has little affect on the velocity, or it can be neglected.

3) The effect of the resistance on the landing velocity

If we loosen the upper gas valve and adjust the lower valve to make the robot land at 0. 267 m/s, then we can obtain three landing curves as shown in Fig. 6(c) after adjusting the value of the resistance (20 Ω, 40 Ω, 60 Ω). The non-resistance curve is the landing velocity obtained after failure of the electricity system.

4. 3 Analysis of experiments

From the above figures, we can conclude that the effect of the electric damper is obvious. If the robot is controlled within 0. 075 to 0. 151 m/s, it can meet the demands of detecting cables. The smaller the resistance is, the slower the landing speed is, which proves the landing theory proposed in section 3.

Fig. 7 shows the spot tests on a cable-stayed bridge in Wuhan, China. The object is the cables A2 to A11 (diameters: 95 to 115 mm; slope angles: 37. 634° to 69. 751°; lengths: 84 to 171 m). The results prove that the robot can be used to inspect the bridge.

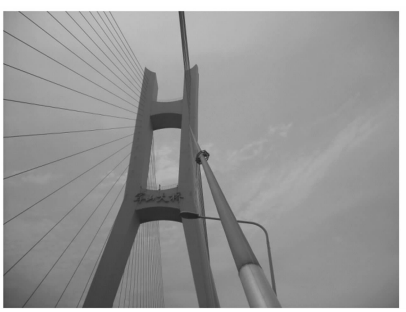

Fig. 7 Field test of the mechanism

According to the theoretical analysis and the experiments, one can conclude that:

1) The robot can climb along the cable slopes any angles.

2) The effect of the electric damper is obvious and it can control the mechanism to land smoothly, but cannot protect the mechanism in the case of electrical system failure.

3) The effect of the upper gas valve can be neglected. We can adjust the lower valve to obtain the landing velocity at 0 to 0. 127 m/s and can alter the value to change the landing speed.

4) Though it is difficult to control, as a mechanical mode with high reliability, the landing mechanism can protect the mechanism from breakage in the case of electricity failure.

5) By adjusting the electric damper based on a gas damper, the satisfactory outcomes that meet the demands of energy-saving landing and safe landing can be obtained.

5 Conclusion and Future Work

In this paper, an innovative wheel-based cable climbing robot that can climb cables with diameters varying from 65 to 205 mm is proposed. Its advantages are small physical volume, simple structure, and high running speed. It can, bearing about 3. 5 kg payloads, move along the cable reliably. Furthermore, using a gas damper and electric damper based on back electromotive force, a landing mechanism is first proposed. The results of both the simulation and the spot tests indicate that the mechanism can guarantee the safe landing of the robot.

References

[1] Bevly D, Dubowsky S, Mavroidis C. A simplified Cartesian computed torque controller for highly geared systems and its application to an experimental climbing robot [J]. *Journal of Dynamic Systems, Measurement and Control*, 2000, **122**(1): 27 – 32.

[2] Baghani A, Ahmadabadi N N, Harati A. Kinematics modeling of a wheel-based pole climbing robot (UT-PCR) [C]//*Proceedings of the* 2005 *IEEE International Conference on Robotics and Automation*(*ICRA*). Barcelona, Spain, 2005: 2111 – 2116.

[3] Luo Jun, Xie Shaorong, Gong Zhenbang. Development of cable maintenance robot for cable-stayed bridges [J]. *Industrial Robot*, 2007, **34**(4): 303 – 309.

[4] Zhang Jialiang, Lü Tiansheng, Luo Jun. Development of arbitrary-gradient cable robot [J]. *High Technology Letters*, 2001, **11**(1): 88 – 90.

[5] Jiang Shengyuan, Han Baoqi, Kang Changji. Application of PLC on cable robot monitoring control system [J]. *Journal of Jilin University*: *Information Science Edition*, 2004, **22**(1): 53 – 56. (in Chinese)

[6] Mehrabi A B, Telang N M, Ghara H. Health monitoring of cable-stayed bridges—A case study[C]//*Proceedings of the* 2004 *Structures Congress—Building on the Past: Securing the Future*. Nashville, TN, USA, 2004: 59 – 66.

[7] Ripin Z M, Soon T B, Abdullah AB, et al. Development of a low-cost modular pole climbing robot[C]//*Proceedings of IEEE Region* 10 *Annual International Conference on TENCON*. Kuala Lumpur, 2000: 196 – 200.

[8] Wang Y, Liu S L, Xu D G, et al. Development and application of wall-climbing robots[C]//*Proceedings of the* 1999 *IEEE International Conference on Robotics and Automation*. Detroit, Michigan, 1999: 1207 – 1212.

[9] Briones L, Bustamante P, Serna M A. Wall-climbing robot for inspection in nuclear power plants[C]//*Proceedings of the* 1994 *IEEE International Conference on Robotics and Automation*. San Diego, CA, USA, 1994: 1409 – 1414.

[10] La R G, Messina M, Muscato G. A low-cost lightweight climbing robot for the inspection of vertical surfaces [J]. *Mechatronics*, 2002, **12**(1): 71 – 96.

[11] White T, Hewer N, Luk N. The design and operational performance of a climbing robot used for weld inspection in hazardous environments[C]//*Proceedings of the* 2005 *IEEE International Conference on Control Applications*. Trieste, Italy, 1998: 451 – 455.

[12] Shen Weimin, Gu Jason, Shen Yanjun. Permanent magnetic system design for the wall-climbing robot[C]//*Proceedings of the* 2005 *IEEE International Conference on Mechatronics and Automation*. Niagara Falls, Canada, 2005: 2078 – 2083.

[13] Luk B L, Cooke D S, Galt S. Intelligent legged climbing service robot for remote maintenance applications in hazardous environments [J]. *Robotics and Autonomous Systems*, 2005, **53**(2): 142 – 152.

[14] Balaguer C, Gimenez A, Padron V M, et al. A climbing autonomous robot for inspection applications in 3D complex environments [J]. *Robotica*, 2000, **18**(3): 287 – 297.

[15] Wang Xingsong, Xu Fengyu. Design and experiments on cable inspection robot [C]//*The* 33*rd Annual Conference of the IEEE Industrial Electronics Society*. Taipei, China, 2007: 2870 – 2875.

[16] Dong Y H, Gao H L, Zhou J E, et al. Evaluation of gas release rate through holes in pipelines[J]. *Journal of Loss Prevention in the Process Industries*, 2002, **15**(6): 423 – 428.

双边轮式斜拉桥悬索检测机器人设计与分析

徐丰羽　王兴松　许家林

(东南大学机械工程学院,南京 211189)

摘要:为了检测斜拉桥圆柱形悬索内部钢丝情况,设计了一种新型的双边轮式悬索爬升机器人,简述了其机械结构及运动方式,建立了爬升模型,分析了其机构的静态特性,并以直径为 139 mm 的悬索为例给出了相关设计参数. 为使机构在电路系统故障时能安全回收,提出了一种基于反电动势理论的安全节能回收方法,应用曲柄滑块驱动气缸设计了气体阻尼机构,以消耗机构下降时因重力作用产生的多余动能,并建立了机构数学模型来仿真下降速度. 试验结果表明,所设计的机器人能携带 3.5 kg 重物沿直径为 65 ~ 205 mm 的悬索平稳运行,满足了悬索检测的实用要求.

关键词:爬升机器人;节能回收;气体阻尼;悬索;斜拉桥

中图分类号:TP242.3